Turkish Journal of Electrical Engineering & Computer Sciences

http://journals.tubitak.gov.tr/elektrik/

Research Article

Turk J Elec Eng & Comp Sci
(2022) 30: 1962 – 1979

doi:10.55730/1300-0632.3916

Prediction of broken rotor bar in induction motor using spectral entropy features and TLBO optimized SVM

Sudip HALDER*, Sunil BHAT, Bimal DORA
Department of Electrical Engineering, Visvesvaraya National Institute of Technology, Nagpur, India

Received: 31.01.2022 • **Accepted/Published Online:** 13.06.2022 • **Final Version:** 22.07.2022

Abstract: The information of the fault frequency characteristics is of great importance for all associated fault diagnostics. This requires a high-resolution spectrum analysis to achieve efficient monitoring of machinery faults, especially while diagnosing rotor bar breakage under light load conditions, because the fault frequencies almost overlap with the fundamental. In this context, rather than looking for frequencies associated with rotor faults, several frequency bands are observed separately in terms of the entropy contained within these bands. First, the motor current signal has been divided into several frequency bands using the continuous wavelet transform (CWT), and the spectral entropy is calculated from each band as the features to describe the rotor condition. Principal component analysis (PCA) has been used as a feature reduction tool, and the features projected onto the first two principal components have been fed into the SVM for inference. SVM is a supervised learning method used for classification and regression analysis. To improve classification performance, a radial basis function (RBF) kernel has been employed, and to find the optimal value of the kernel parameters, a metaheuristic approach, namely teaching learning-based optimization (TLBO), is utilized. The ANSYS 2D workbench is used to simulate the finite element model (FEM) of an induction motor with broken rotor bars, and the efficacy of the proposed method is then tested using simulated data. To investigate the robustness of the proposed approach, white Gaussian noise has also been added to the simulated data, and the performance of the SVM is tested with these spectral features.

Key words: Broken rotor bar fault, continuous wavelet transform, spectral entropy features, teaching learning-based optimization, support vector machine

Nomenclature

L_b	: Lower bound	ξ	: Constant, governing the clasification error margin
U_b	: Upper bound	L_d	: Dual of the primal SVM optimization problem
N_p	: Population	α	: Lagrange multiplier
T	: Maximum number of iteration	σ	: RBF kernel parameter
X_{best}	: Best solution	ψ	: Mother wavelet
f_i	: Fitness of ith member of population	s	: Scale (Dilation parameter)
T_f	: Teaching factor (either 1 or 2)	C_ψ	: Admissibility constant
r	: Random variable between zero and one	H	: Spectral entropy
C	: Regularization parameter	H_n	: Normalized spectral entropy

*Correspondence: sudip.eie@gmail.com

1. Introduction

Among different induction motor faults, approximately 5%–10% cases are related to the broken rotor bar (BRB) failure [1]. Though broken rotor bar fault is not common as bearing or insulation failure, but can cause terrible destruction in electrical machines. It might happen due to manufacturing imperfections, frequent starting, mechanical and thermal stress, etc., and especially in large motors it can be extremely dangerous. Thus, prevention of this fault has also become a major concern in the field of motor condition monitoring. However, insufficient detection accuracy in broken rotor bar fault diagnosis has inspired many researchers in improving this method. Use of sensors has been shown to be effective for the detection of BRB faults. Hall sensors based magnetic flux assessment [2], infrared image analysis [3], smart sensor based current and vibration analysis [4] has been employed efficiently for rotor condition monitoring. The oscillatory behavior of motor torque is also a good indication of rotor fault. Therefore, with the help of a torque sensor electromagnetic torque has been analyzed [5] in the frequency domain to estimate rotor health. But the main drawback of these approaches is the use of costly sensors and necessary hardware with them. Several parameter estimation methods have been proposed to estimate the parameters which cannot be measured easily. Air gap torque estimation [6], Kalman filter-based flux estimation [7] are some of the good examples of BRB fault detection techniques. Being a noninvasive technique motor current signature analysis (MCSA) [8–10] based methodologies are becoming dominant for years which can avoid the need of extra hardware complexity. Most of the current analysis methods consist of finding sideband frequency components (SFCs) corresponding to the fault. But the problem is that these SFCs are very closely spaced components and the conventional spectral analysis approach does not have the necessary resolution to identify these components, hence high-resolution spectral analysis techniques have been used to meet the purpose. Multiresolution Taylor–Kalman approach [11], Prony analysis [10], and root-MUSIC analysis [12] have been shown to be good solutions for the spectral resolution problems. It is also advantageous to analyze the current envelope [13] i.e. how the phase current is being modulated due to fault. But detecting the current envelope is difficult in practical cases when noises are present in the recorded signal. Analysis of current features in the time-frequency domain has also been proven to be a good diagnostic mechanism for machinery fault analysis. In this regard more specifically the startup transient analysis of stator current has been investigated. The analysis lies on the exposure of a V pattern in the time-frequency plane produced by the evolution of sidebands corresponding to rotor fault. Positive outcomes have been found through the approaches based on Hilbert transform [14], Hilbert–Huang transform [15], Gabor analysis [15, 16], complex empirical mode decomposition (EMD) [17], synchrosqueezing transform [18], short-time Fourier transform (STFT) [19]. In general, machinery faults result in a magnetic asymmetry in the air gap. To investigate this asymmetry search coil-based techniques have been proposed where search coils are wound around the stator teeth to capture the air gap flux for further analysis [20]. Not only air gap flux, but stray flux signature analysis (SFSA) can also be employed for health assessment of rotor bar [21]. This method of stray flux analysis is also competing with the conventional MCSA approaches as it has been successfully applied on numerous machinery faults [22–24]. Despite the availability of advanced methods, several cases of false alarms have been reported [25, 26] which is undesirable and it eventually leads to the use of artificial intelligence and machine learning-based approaches which are proven to be very effective specifically when multiple fault diagnosis is required. In this context, some of the mentionable works are based on fuzzy logic [27], hybrid FMM–CART model [28], convolution neural network(CNN) [29], which have been used as an effective diagnostic tool to detect faults like broken rotor bar, eccentricity problems, unbalanced voltage, bearing failure, etc. Though neural network-based diagnosis schemes are very efficient, particularly for online fault detection, they have several drawbacks, which are as follows:

- Optimal tuning of network parameters is difficult due to the huge number of parameters that must be optimized.
- The learning process is time-consuming due to the high computational burden.
- Sometimes it gets stuck on local optima, affecting overall effectiveness.

Also in the case of fuzzy logic-based approaches, finding optimized membership functions requires good domain expertise. SVM, on the other hand, is preferred [30] because it requires only the support vectors, which are very few in total datasets, leading to a high training speed of the model. Even in cases of linearly inseparable features, SVM performs efficiently using kernel tricks [31]. Choice of optimal parameters can also be done easily based on the crossvalidation score. For this purpose, TLBO has been used because it is robust and involves comparatively less computational effort compared to other metaheuristic approaches. With all of the previously mentioned benefits, the authors used SVM as a rotor fault prediction tool. The proposed method consists of three steps. First, using CWT-based signal reconstruction, spectral entropy features are extracted from the stator current signal. Second, suitable SVM parameters were chosen using teaching learning-based optimization (TLBO) to improve the accuracy of the 10-fold crossvalidation performance. Finally, the trained SVM model is used to predict broken rotor bars in the induction motor. The following are the primary contributions of this work:

- FEM simulation and study of broken rotor bar fault in an induction motor.
- Application of FFT-based CWT to resolve the current signal in different frequency bands.
- New features based on spectral entropy in different frequency bands are extracted from the current signal.
- Tuning of SVM hyperparameters using TLBO algorithm and prediction of rotor faults.

The next section provides a thorough theoretical foundation for the proposed method, which includes the basics of SVM, parameter tuning using TLBO, feature extraction mechanism, computation of spectral entropy, choice of mother wavelet and feature reduction using PCA.

2. Theoretical background

2.1. Basics of support vector machine (SVM)

The classifier is trained to find a hyperplane by applying the margin maximization principle to feature vectors that can optimally separate two classes.

A hyperplane (linear discriminant function) g(x) = W.X+b is defined (Figure 1) to separate the classes, where W is a weight vector which is perpendicular to the hyperplane, and b is an offset. The hyperplane is found by solving the optimization problem as follows [32]:

$$f(W,\xi) = \begin{cases} \min\limits_{W} \frac{1}{2}|W|^2 + C\left(\sum_{i=1}^{l}\xi_i\right) \\ s.t.\ \ Y_i(W.X_i + b) \geq 1 - \xi_i, \qquad \xi_i \geq 0 \ \ \forall i \end{cases} \tag{1}$$

Here, l is number of training set, C represents the regularisation parameter, and ξ is a constant that governs the classification margin of error. The input vector is denoted by X, and Y represents the output classes. The

following dual can be used to find the solution to (1) [33].

$$\begin{cases} maxL_d = \sum_i \alpha_i \alpha_j Y_i Y_j K(X_i X_j) \\ s.t.\ \ 0 \le \alpha_i \le C \ \ \forall i, \qquad \sum_i \alpha_i Y_i = 0 \end{cases} \tag{2}$$

$K(X_i X_j)$ denotes a nonlinear kernel function. If the feature points are not linearly separable kernel functions are used for mapping the data to higher dimensional feature space ϕ, where the points become linearly separable. The discriminant function g(x) then becomes

$$g(x) = W^T \phi(X) + b \tag{3}$$

$$= \sum_{s \in SV} \alpha_i \phi(X_i)^T \phi(X_i) + b. \tag{4}$$

A kernel function K is defined as a function that corresponds to a dot product of two feature vectors in some expanded feature space,

$$K(X_a, X_b) = \phi(X_a).\phi(X_b). \tag{5}$$

Most commonly used kernel functions are:

$$Linear\ K(X_i, X_j) = X_i.X_j \tag{6}$$

$$Polinomial\ of\ power\ p \quad K(X_i, X_j) = (1 + X_i.X_j)^p \tag{7}$$

$$Radial\ basis\ function \quad K(X_i, X_j) = e^{-\frac{||X_i - X_j||^2}{2\sigma^2}}. \tag{8}$$

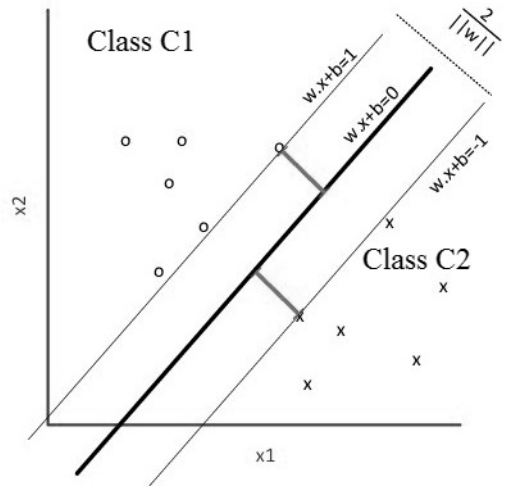

Figure 1. SVM classifier.

According to the aforementioned mathematical analysis, SVM was designed primarily for binary classification. As a result, SVM is further modified to address multiclassification issues. A multiclass SVM can be created by combining several binary classifiers. To generate multiclass SVM, two techniques are mostly used: One-vs-One (OVO) and One-Vs-Rest (OVR). These techniques determine the algorithm's speed and accuracy. The authors have used the OVR technique to achieve greater accuracy in this work.

2.1.1. Parameter tuning for SVM Kernel

When using the RBF kernel, there are primarily two parameters to optimize: regularisation (C) and sigma (σ) before conducting the final training and testing procedure. Many studies attempted to find SVM parameters empirically by attempting a limited number of values and retaining the values that produced the best results. However, in order to find viable solutions, this procedure necessitates a thorough search of the entire search space. A grid search was used to look for ways to optimize SVM parameters in the parameter space, where the parameters change with a fixed step size [34]. Applications of particle swarm optimization (PSO) [35], genetic algorithm (GA) [36], and ant colony optimization (ACO) [37] are also noteworthy in this context. The authors used the teaching learning-based optimization (TLBO) method, which was proposed by Rao et al. [38], because it finds global optima quickly with little computational effort and has a high consistency. In this work, parameter tuning is done on the Python-3 platform.

2.1.2. TLBO

This method focuses on the impact of the teacher's influence on students. The process is divided into two parts: the first is the "teacher phase", in which new solutions are generated using the best solution and the population mean. If the new solution is superior to the current one, it is accepted (greedy selection). The second phase is known as the "learner phase", and it involves the creation of a new solution using a partner solution. Acceptance of this solution is based on the same greedy selection strategy as before. The goal of TLBO is to improve the performance of SVM, and classification accuracy has been used as a performance metric in this context. For a test data set, the accuracy can be given as:

$$Accuracy = \frac{TP + TN}{TP + FP + TN + FN}. \tag{9}$$

Here TP: True positive, FP: False positive, TN: True negative and FN: False negative. Because the authors used 10-fold crossvalidation, accuracy has been measured for all ten iterations, and the average accuracy has been used as the SVM's performance parameter.

$$Accuracy_{ave} = \sum_{i=1}^{10} Accuracy \tag{10}$$

Finally to implement TLBO, the fitness function is defined as (1-$accuracy_{ave}$), which must be minimised using the best SVM parameters. Figure 2 depicts the TLBO pseudocode and the proposed tuning approach for SVM parameters.

2.2. Feature extraction

2.2.1. Resolving the signal into different frequency bands using CWT

The two common methods for computing wavelet coefficients are the convolution-based algorithm and the FFT-based algorithm [39]. Considering the mother wavelet as $\psi(t)$ CWT coefficients as per the first method for a time location τ can be given as

$$T_x(\tau, s) = (x * \bar{\psi}_s)(\tau), \tag{11}$$

where $\bar{\psi}_s = \frac{1}{\sqrt{s}}\psi^*(\frac{-t}{s})$. The computation starts at $\tau = 0$, and τ is to be incremented until the end of the signal is reached. The calculation of CWT coefficients has to be done for each time step.

Input: Fitness function, L_b, U_b , N_p, T
Initiate random population (P)
Evaluate fitness of P
for t=1 to T

for i=1 to N_p
Choose X_{best}
Determine X_{mean}
$X_{new} = X_i + r\,(X_{best} - T_f\,X_{mean})$
Bound X_{new} and evaluate it's fitness f_{new}
Accept X_{new} if it is better than X_i

Choose any solution X_p randomly
Determine X_{new} as:
if $f_i < f_p$
$X_{new} = X_i + r\,(X_i - X_p)$
else
$X_{new} = X_i - r\,(X_i - X_p)$
end
Bound X_{new} and evaluate it's fitness f_{new}
Accept X_{new} if it is better than X_i
end
end

(a) Pseudocode of TLBO.

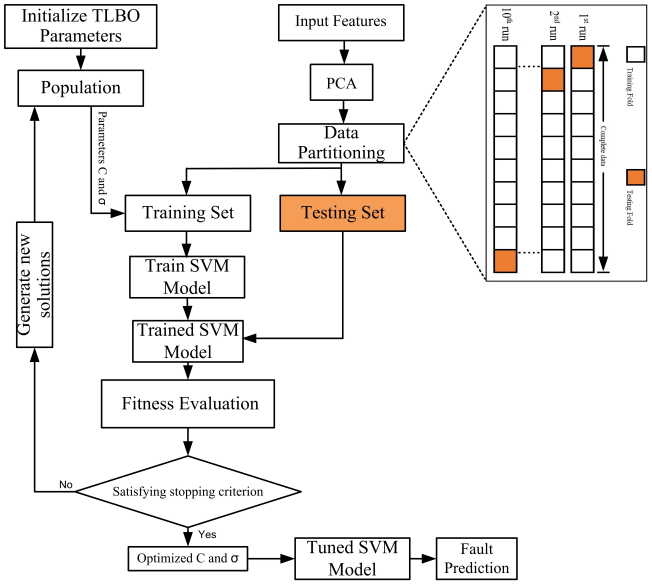

(b) Application of TLBO for SVM parameter tuning.

Figure 2. Tuning of SVM hyperparameters.

The FFT-based wavelet transform, on the other hand, does not require the inner loop computation related to the translation parameter (τ), making it more computationally efficient than the first. Wavelet transform in with this method can be given as

$$T_x(\tau, s) = \int_{-\infty}^{\infty} x(t)\psi^*_{\tau,s}(t)dt \tag{12}$$

$$= \int_{-\infty}^{\infty} x(t)\frac{1}{\sqrt{s}}\psi^*(\frac{t-\tau}{s})dt, \tag{13}$$

where τ and s are translation and dilation parameter (scale), respectively. Recovery of the signal is possible with the wavelet transform coefficients using the equation below

$$x(t) = \frac{1}{C_\psi}\int_{-\infty}^{\infty}\int_{0}^{\infty} T_x(\tau, s)\psi_{\tau,s}(t)\frac{1}{s^2}dsd\tau. \tag{14}$$

Here C_ψ is defined as $\int_0^\infty \frac{\psi^*_\omega \psi_\omega}{\omega}d\omega$. For both these analysis and synthesis purpose the wavelet should satisfy the zero average condition i.e. $\int_{-\infty}^{\infty}\psi(t)dt = 0$ and the admissibility condition i.e. $C_\psi < \infty$. Fourier Transform of the CWT along the dimension τ can be written as

$$\mathcal{F}[T_x(\tau, s)] = \sqrt{s}X(\omega)\psi^*(s\omega). \tag{15}$$

Now taking the inverse the CWT coefficients can be given as

$$T_x(\tau, s) = \frac{1}{2\pi} \int_{-\infty}^{\infty} \sqrt{s} X(\omega) \psi^*(s\omega) e^{j\omega\tau} d\tau. \tag{16}$$

Here CWT is evaluated at all values of τ in a single run for particular value of scale parameter, hence this FFT based approach is computationally efficient. The signal corresponding to each scale can be reconstructed as per equation (12). Since each scale represents a different bandpass filter, the input signal can be resolved into multiple signals with varying frequency contents based on the filter represented by those scales. Finally, spectral entropy has been calculated for each reconstructed signal as a feature to be fed into the SVM model. The following subsection discusses the computational aspects of spectral entropy.

2.2.2. Computation of spectral entropy

A signal's spectral entropy (SE) is an assessment of its spectral power distribution. It computes the Shannon entropy considering the normalized power distribution of the signal in the frequency domain as a probability distribution. This feature can be used for machinery damage investigation [40]. Given X(k) as the DFT of the signal x(n), the power spectral density of the signal is:

$$S(k) = |X(k)|^2. \tag{17}$$

Then the probability distribution P(k):

$$P(k) = \frac{S(k)}{\sum_i S(i)}. \tag{18}$$

And the spectral entropy can be given as

$$H = -\sum_{k=1}^{M} P(k) log_2 P(k). \tag{19}$$

Finally the normalized spectral entropy:

$$H_n = -\frac{\sum_{k=1}^{M} P(k) log_2 P(k)}{log_2 N}. \tag{20}$$

Here M is the number of frequency points. Figure 3 depicts the entire method of the proposed feature extraction.

2.2.3. Choice of mother wavelet

When performing CWT-based analysis, the choice of mother wavelet is equally significant because it depends on the application and also the data to be studied. Orthogonal wavelet families (such as Haar wavelet) and nonorthogonal wavelet families (such as Morlet wavelet, Gaussian wavelet, Paul wavelet) are mostly common among diverse wavelet families [41]. In the field of time-series analysis, nonorthogonal wavelets are highly prevalent. The morlet wavelet, in particular, is very beneficial in this context because of its efficiency in extracting oscillatory features from the signal. The expression for this wavelet can be given as

$$\psi_x = Ce^{-x^2} cos(5x). \tag{21}$$

The constant C is used for normalization while reconstructing the signal. The benefits [42] listed below are the main reasons for using this wavelet to calculate CWT coefficients.

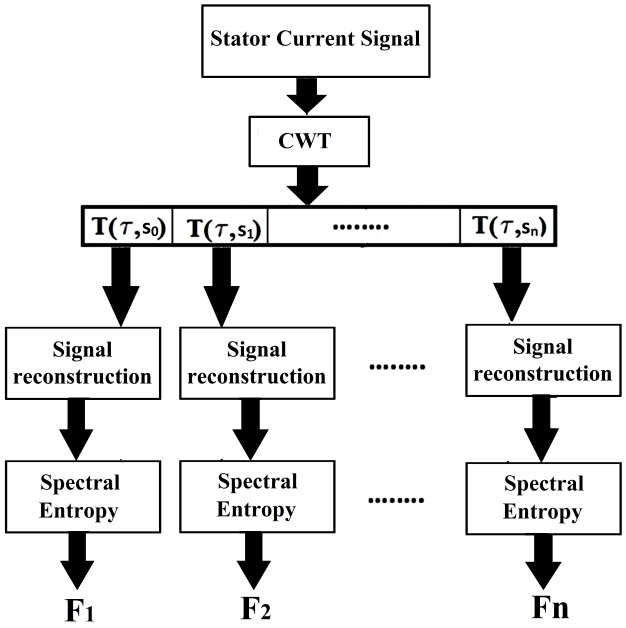

Figure 3. Proposed feature extraction.

- The Morlet wavelet is Gaussian-shaped in the frequency domain, which minimises signal ripple effects.
- Compared to other methods, wavelet convolution is more computationally efficient and requires less code.

2.3. Feature reduction with PCA

Principal component analysis (PCA) evaluates most meaningful linear projection of original features on a new basis that maximizes the scatter of all projected features. For a feature vector X, which is a (m x n) matrix where m is the number of features and n is number of data trials. A new feature vector Y is defined by linear transformation Y = P.X, where P is a matrix of orthogonal rows representing the basis of new feature space. Defining the covariance matrix of Y, $S_Y = \frac{1}{(n-1)}$ Y.Y^T the main goal of PCA is to diagonalize S_Y which means the new features are completely uncorrelated.

$$\begin{aligned} S_Y &= \frac{1}{(n-1)} Y.Y^T \\ &= \frac{1}{(n-1)} (PX).(PX)^T \\ &= \frac{1}{(n-1)} PX.X^T P^T \\ &= \frac{1}{(n-1)} PAP^T, \end{aligned}$$

where A = XX^T is a symmetric matrix. From theory of linear algebra matrix A can be diagonalized as A = MDM^T, where D is a diagonal matrix and M is a matrix of eigenvectors of A. Now if P is chosen such that P

$= M^T$ then A $= P^T$DP. Substituting this to the equation of S_Y,

$$S_Y = \frac{1}{(n-1)} P(P^T DP)P^T$$
$$= \frac{1}{(n-1)} (PP^T)D(PP^T).$$

As M is an orthogonal matrix so as P. Hence PP^T = PP^{-1}=I and S_Y can be written as

$$S_Y = \frac{1}{(n-1)} D.$$

Clearly S_Y is now diagonalized and ith diagonal value of S_Y is the variance of X along P_i, where P_i is ith principal component of X. In this paper first two principal components have been taken for classification. The study of rotor fault using FEM of an induction motor is described in the following section.

3. FEM simulation of BRB fault

Broken rotor bar (BRB) fault is implemented on a machine with the data as shown in Table 1, in ANSYS Maxwell 2D. The fundamental equation relating time and space variations of the vector potential over the section to be analyzed is given as [43]

$$D : \frac{\partial}{\partial x}(\frac{1}{\mu}\frac{\partial A_z}{\partial x}) + \frac{\partial}{\partial y}(\frac{1}{\mu}\frac{\partial A_z}{\partial y}) = -J_z + \sigma\frac{\partial A_z}{\partial t}$$

$$\Gamma_1 : A_z = 0.$$

Here D is the analysis area, Γ_1 is the outside peripheral of stator and inside peripheral of the rotor (the Dirichlet boundary conditions). The current density is denoted as J_z and the conductivity of a conductor is σ. Permeability is denoted as μ and A_z indicates the magnetic vector potential.

As because of broken rotor bar current cannot flow through that bar, it tries to flow through adjacent bars which causes field saturation in that area as shown in Figure 4b.

In the subsequent section, the findings obtained utilizing the proposed method for rotor fault diagnostics are explained in detail.

4. Results and discussion

In this work, CWT has been used as a collection of several bandpass filters. The signal recovered from the coefficients corresponding to a particular scale contains a specific band of frequencies having a centre frequency as shown in Table 2. CWT is performed over a predefined set of scales, while the thumb rule for choosing the smallest scale is $s_0 = 2T_0$, where T_0 is the sampling period. With a sampling period of 0.0002 (sampling frequency of 5000), the smallest scale taken is 0.0004. Considering N to be the total number of samples of an input signal, the total number of scales is given as

$$N_{sc} = nearest\ integer\ of\ \frac{log_2 N \times T_0/s_0}{\delta_s}. \tag{22}$$

Table 1. Motor specification.

Given output power (HP)	1
Rated voltage (V)	220
Number of poles	4
Frequency (Hz)	60
Number of stator slots	48
Number of rotor slots	34
Air gap (mm)	0.35
Stator resistance R1 (ohm)	2.59627
Stator leakage reactance X1 (ohm)	3.66015
Rotor resistance R2 (ohm)	2.57657
Rotor leakage reactance X2 (ohm)	7.89809
Magnetizing reactance Xm (ohm)	274.656
Efficiency (%)	88.2029
Power factor	0.929495

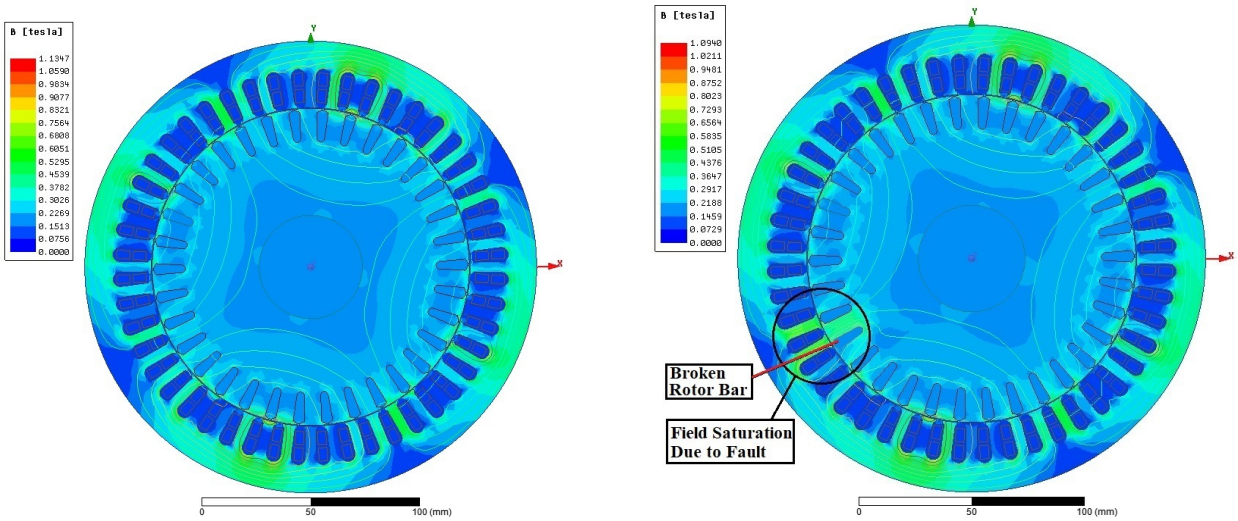

Field distribution at healthy condition. Field distribution with one broken bar

Figure 4. FEM simulation of broken bar fault.

Here δ_s is spacing between two scales and taken as 0.4875. Finally the scales are chosen in a dyadic manner and the ith scale can be given as

$$s_i = s_0 \times 2^{i \times \delta_s} \quad i = 0 \; to \; (N_{sc} - 1). \tag{23}$$

As a length of 2000 samples has been considered for extracting the fault features, N_{sc} comes out to be 20. Total 20 scales (computed as Equation 22) and the corresponding center frequencies are given in Table 2.

The signal corresponding to individual scales has been reconstructed by zeroing out the coefficients related to other scales after the CWT coefficients for all scales have been computed. "Hard thresholding" is another name for this technique. The spectral entropy of each reconstructed signal was then calculated to extract 20 features, denoted as F1 to F20. A total of 600 feature samples were extracted for the motor under two different loading conditions (no load and medium load). One sample for each case has been given in Table 3.

Table 2. Scales and corresponding center frequencies.

0.0004	3978.873577	0.002166809	734.5130663	0.011737652	135.5935126	0.06358312	25.03100558
0.000560805	2837.971419	0.003037895	523.8987992	0.016456343	96.71343055	0.089144378	17.85361536
0.000786256	2024.211531	0.004259169	373.6760643	0.023072012	68.98182273	0.1249816	12.73426992
0.001102342	1443.789143	0.005971411	266.5281944	0.032347267	49.20197577	0.175225861	9.082845531
0.001545498	1029.797063	0.008371998	190.1039034	0.045351297	35.09380187	0.245668982	6.478430521

Table 3. Feature samples.

Healthy	0.795636	0.838671	0.889698	0.907175	0.859875	0.811117	0.753149	0.732723	0.669547	0.645753	0.516324	0.511087	0.510865	0.510851	0.510836	0.524709	0.458323	0.439961	0.430159	0.420574
One BRB	0.802662	0.849932	0.895311	0.846574	0.856536	0.821799	0.766885	0.640968	0.565514	0.673002	0.514066	0.510852	0.510844	0.510844	0.510811	0.533713	0.447577	0.430288	0.420938	0.417195
Two BRB	0.786564	0.853457	0.899143	0.85949	0.862174	0.828597	0.718904	0.629912	0.559766	0.670983	0.51403	0.510905	0.510876	0.510879	0.510924	0.536199	0.436022	0.42627	0.41873	0.417211
Healthy	0.792869	0.840174	0.896497	0.905737	0.85937	0.812827	0.764386	0.720876	0.676434	0.644799	0.515167	0.510891	0.510819	0.510813	0.510835	0.527311	0.461865	0.44298	0.429703	0.419961
One BRB	0.789041	0.84324	0.900218	0.884983	0.866002	0.829374	0.760108	0.62712	0.558765	0.674712	0.513866	0.510808	0.510805	0.510802	0.510737	0.532915	0.437331	0.4267	0.41917	0.415363
Two BRB	0.801363	0.8485	0.897878	0.843656	0.847642	0.814973	0.727194	0.592962	0.534028	0.649177	0.516545	0.510945	0.51082	0.51082	0.510901	0.52981	0.461755	0.436386	0.428263	0.422714

PCA has been used to reduce the number of features. Feature reduction helps to avoid overfitting and also leads to better human interpretations and lower computational costs. PCA builds new independent features from old features and a combination of both, eliminating correlated variables that do not contribute to any decision making. Features from the first two principal components have been used to predict rotor faults. Before those features are fed, the multiclass SVM classifier has been tuned using the TLBO technique. Based on the accuracy of 10-fold crossvalidation, optimal C and sigma were chosen. Figure 5 shows that convergence occurs after 75 iterations with best fitness value = 0.013333. The best parameters obtained as, c = 91.15518313 and σ = 9.78368304. A population size of 50 has been chosen for optimization, and the algorithm has been run for 200 iterations.

Figure 6 shows the classification using this tuned SVM for both no load and medium load cases. Though faulty features are always distinguished from healthy ones, distinguishing one broken rotor bar from two broken rotor bars is relatively difficult in a no load situation. However, the RBF kernel has taken care of this issue admirably. On the other hand, when the load increases (medium load), these characteristics become more distinct.

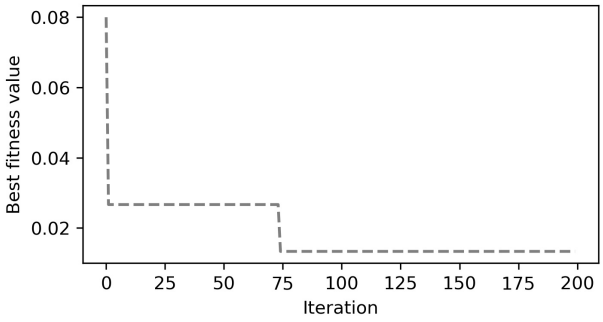

Figure 5. Convergence curve of TLBO.

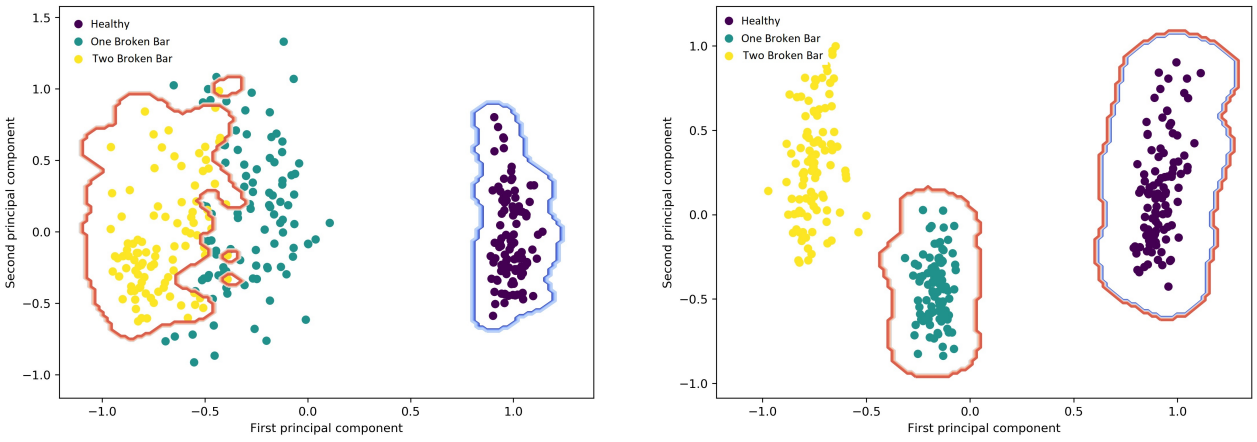

No load condition. Medium load condition.

Figure 6. Classification with decision boundary.

The receiver operating characteristic (ROC) curve has been shown in Figure 7 as a performance measure for the SVM classifier. The rate of true positives vs. false positives is represented by the ROC curve. The performance of classifiers with curves closer to the top-left corner is superior. Figure 7a shows that for the no

load condition, the ROC curve is perfect only for the case of healthy vs. rest, but SVM cannot achieve a true positive rate of 100 percent with zero false positives in the other two situations (one BRB vs rest and two BRB vs rest). However, as the load rises, the classification accuracy increases to 100%, as illustrated in Figure 7b. Hence the proposed approach can separate the faulty machine fairly easily, even at no load condition, but the accuracy reduces while distinguishing machines with 1 BRB and 2 BRB. But, with a loaded machine, all the faulty and healthy situations are well separated.

On the basis of precision, recall, and f1-score, the authors compared the classification performance with that of other commonly used machine learning (ML) approaches, such as logistic regression (LR), k-nearest neighbor (KNN), and naive Bayes (NB). Table 4 shows the comparative analysis for no load situation where accuracy is higher for SVM.

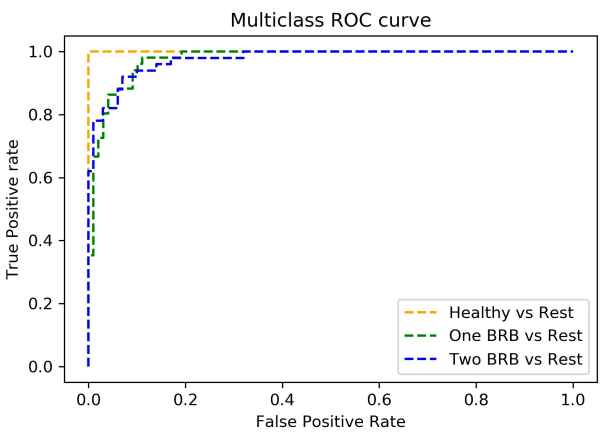

No load condition.

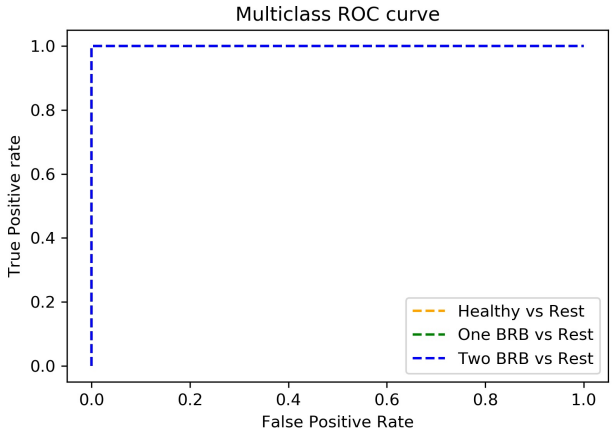

Medium load condition.

Figure 7. Multiclass ROC curve.

Table 4. Comparison with other ML methods.

SVM					LR				
	Precision	Recall	F1-score	Support		Precision	Recall	F1-score	Support
Healthy	1	1	1	49	Healthy	1	1	1	47
One BRB	0.87	0.88	0.87	51	One BRB	0.82	0.74	0.78	54
Two BRB	0.88	0.86	0.87	50	Two BRB	0.74	0.82	0.78	49
Accuracy			0.91	150	Accuracy			0.85	150
Macro avg	0.91	0.91	0.91	150	Macro avg	0.85	0.85	0.85	150
Weighted avg	0.91	0.91	0.91	150	Weighted avg	0.85	0.85	0.85	150
KNN					NB				
	Precision	Recall	F1-score	Support		Precision	Recall	F1-score	Support
Healthy	1	1	1	47	Healthy	1	1	1	47
One BRB	0.82	0.87	0.85	54	One BRB	0.83	0.83	0.83	54
Two BRB	0.85	0.8	0.82	49	Two BRB	0.82	0.82	0.82	49
Accuracy			0.89	150	Accuracy			0.88	150
Macro avg	0.89	0.89	0.89	150	Macro avg	0.88	0.88	0.88	150
Weighted avg	0.89	0.89	0.89	150	Weighted avg	0.88	0.88	0.88	150

After the SVM model has been trained, it is tested on 150 randomly selected samples to see how well it predicts. Figure 8 depicts the resulting confusion matrix. In the no load situation, a few samples are misclassified, but with loading, the SVM model has shown 100% accuracy. The proposed method's performance is also compared to that of recently reported relevant methods, as shown in Table 5.

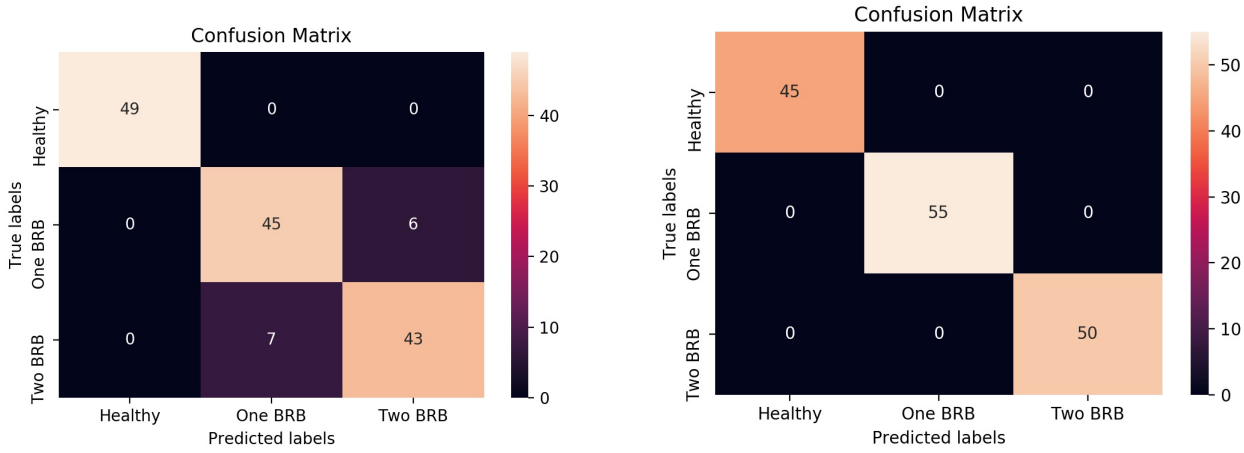

No load condition. Medium load condition.

Figure 8. Confusion matrix.

Table 5. Proposed methodology performance comparison.

Reference	Method	Detected fault	Analysed signal	Motor state	Accuracy rate
Aydin et al. [44]	Hilbert transform, boundary analysis and Fuzzy decision tree	1 BRB 2 BRB	Current signal	Steady state	98.75
Weiguo Zhao et al. [45]	PCA and multivariate relevance vector machine with multiple Gaussian kernels	v1 BRB 2 BRB 3 BRB	Current signal	Steady state	80-95
Weiguo Zhao et al. [46]	Fuzzy logic approach based on contrast computation	1 BRB 2 BRB	Current signal	Steady state	98.30
Rangel Magdaleno et al. [47]	Hilbert transform and statistical analysis	0.5 BRB 1 BRB 1.5 BRB	Current signal	Start up transient	99
Proposed	Spectral entropy and tuned SVM	1 BRB 2 BRB	Current signal	Start up transient	91-100

5. Severity estimation

The approximate entropy of the current signal has been computed for quantitative analysis of fault severity. The fault harmonics in the signal increase as the number of broken rotor bars increases, resulting in higher approximate entropy. As a result, it is a good choice for estimating fault severity. Figure 9 shows how it changes as the number of broken bars increases.

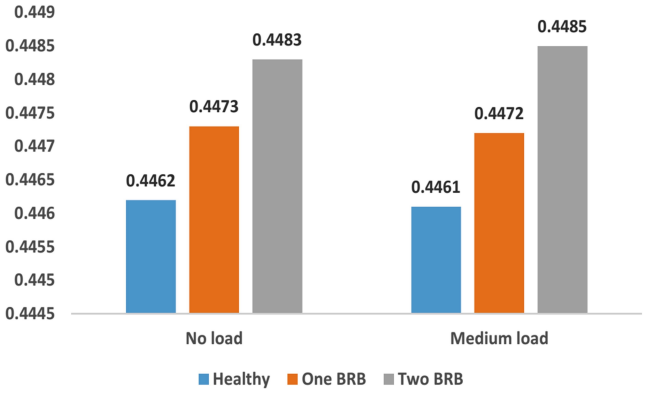

Figure 9. Fault severity estimation.

6. Conclusion and future works

This paper proposes new frequency domain features derived from various frequency bands for the precise prediction of rotor fault in an induction motor. The main goal of using CWT is to filter the current signal with several bandpass filters with the least amount of computation. Individual filtered signals are then subjected to spectral entropy computation and treated as features for fault detection. When the proposed features are combined with SVM, with optimally chosen parameters, they result in precise fault detection. According to the findings, the proposed method is capable of accurately predicting rotor faults while having low computational complexity. The proposed scheme has also been tested under two different loading conditions and at different fault severity levels. The presented feature extraction technique is validated by combining it with KNN, LR and NB in order to justify the effectiveness of the TLBO optimized SVM model compared to other commonly used ML approaches. Though the proposed method is extremely effective in predicting rotor faults, it cannot be used in the situation of an inverter-fed motor running at a very low speed because fault frequencies are strongly related to the slip, which is determined by the motor speed. In such circumstances, a new set of training data must be obtained, and the SVM should be trained with that data set to generate accurate results.

Future research could go in a number of directions. To begin, the proposed approach can be validated using the current signal from a real experimental setup. Second, other metaheuristic algorithms' performance can be evaluated in order to fine-tune SVM parameters. Finally, the approach's effectiveness can be tested by looking into other machine faults like irregular air gaps, stator interturn failure, and so on.

References

[1] Zhang P, Du Y, Habetler TG, Lu B. A survey of condition monitoring and protection methods for medium-voltage induction motors. IEEE Transactions on Industry Applications 2010; 47 (1): 34-46. doi: 10.1109/TIA.2010.2090839

[2] Dias CG, Chabu IE. Spectral analysis using a Hall effect sensor for diagnosing broken bars in large induction motors. IEEE Transactions on Instrumentation and Measurement 2014; 63 (12): 2890-2902. doi: 10.1109/TIM.2014.2328184

[3] Resendiz-Ochoa E, Osornio-Rios RA, Benitez-Rangel JP, Romero-Troncoso RD, Morales-Hernandez LA. Induction motor failure analysis: An automatic methodology based on infrared imaging. IEEE Access 2018; 6: 76993-77003. doi: 10.1109/ACCESS.2018.2883988

[4] Luong P, Wang W. Smart sensor-based synergistic analysis for rotor bar fault detection of induction motors. IEEE/ASME Transactions on Mechatronics 2020; 25 (2): 1067-1075. doi: 10.1109/TMECH.2020.2970274

[5] Gyftakis KN, Spyropoulos DV, Kappatou JC, Mitronikas ED. A novel approach for broken bar fault diagnosis in induction motors through torque monitoring. IEEE Transactions on Energy Conversion 2013; 28 (2): 267-277. doi: 10.1109/TEC.2013.2240683

[6] da Silva AM, Povinelli RJ, Demerdash NA. Rotor bar fault monitoring method based on analysis of air-gap torques of induction motors. IEEE Transactions on Industrial Informatics 2013; 9 (4): 2274-2283. doi: 10.1109/TII.2013.2242084

[7] Eltabach M, Charara A, Zein I. A comparison of external and internal methods of signal spectral analysis for broken rotor bars detection in induction motors. IEEE Transactions on Industrial Electronics 2004; 51 (1): 107-121. doi: 10.1109/TIE.2003.822083

[8] Benbouzid ME. A review of induction motors signature analysis as a medium for faults detection. IEEE transactions on industrial electronics 2000; 47 (5): 984-993. doi: 10.1109/41.873206

[9] Pires VF, Kadivonga M, Martins JF, Pires AJ. Motor square current signature analysis for induction motor rotor diagnosis. Measurement 2013; 46 (2): 942-948. doi: 10.1016/j.measurement.2012.10.008

[10] Chen S, Živanović R. Estimation of frequency components in stator current for the detection of broken rotor bars in induction machines. Measurement 2010; 43 (7): 887-900. doi: 10.1016/j.measurement.2010.03.006

[11] Trujillo-Guajardo LA, Rodriguez-Maldonado J, Moonem MA, Platas-Garza MA. A multiresolution Taylor–Kalman approach for broken rotor bar detection in cage induction motors. IEEE Transactions on Instrumentation and Measurement 2018; 67 (6): 1317-1328. doi: 10.1109/TIM.2018.2795895

[12] Trachi Y, Elbouchikhi E, Choqueuse V, Benbouzid ME. Induction machines fault detection based on subspace spectral estimation. IEEE Transactions on Industrial Electronics 2016; 63 (9): 5641-5651. doi: 10.1109/TIE.2016.2570741

[13] Sapena-Bano A, Pineda-Sanchez M, Puche-Panadero R, Martinez-Roman J, Kanović Ž. Low-cost diagnosis of rotor asymmetries in induction machines working at a very low slip using the reduced envelope of the stator current. IEEE Transactions on Energy Conversion 2015; 30 (4): 1409-1419. doi: 10.1109/TEC.2015.2445216

[14] Pineda-Sanchez M, Riera-Guasp M, Antonino-Daviu JA, Roger-Folch J, Perez-Cruz J et al. Instantaneous frequency of the left sideband harmonic during the start-up transient: A new method for diagnosis of broken bars. IEEE Transactions on Industrial Electronics 2009; 56 (11): 4557-4570. doi: 10.1109/TIE.2009.2026211

[15] Antonino-Daviu JA, Riera-Guasp M, Pineda-Sanchez M, Perez RB. A critical comparison between DWT and Hilbert–Huang-based methods for the diagnosis of rotor bar failures in induction machines. IEEE Transactions on Industry Applications 2009; 45 (5): 1794-1803. doi: 10.1109/TIA.2009.2027558

[16] Riera-Guasp M, Pineda-Sanchez M, Pérez-Cruz J, Puche-Panadero R, Roger-Folch J et al. Diagnosis of induction motor faults via Gabor analysis of the current in transient regime. IEEE Transactions on Instrumentation and Measurement 2012; 61 (6): 1583-1596. doi: 10.1109/TIM.2012.2186650

[17] Georgoulas G, Tsoumas IP, Antonino-Daviu JA, Climente-Alarcón V, Stylios CD et al. Automatic pattern identification based on the complex empirical mode decomposition of the startup current for the diagnosis of rotor asymmetries in asynchronous machines. IEEE Transactions on Industrial Electronics 2013; 61 (9): 4937-4946. doi: 10.1109/TIE.2013.2284143

[18] Camarena-Martinez D, Perez-Ramirez CA, Valtierra-Rodriguez M, Amezquita-Sanchez JP, de Jesus Romero-Troncoso R. Synchrosqueezing transform-based methodology for broken rotor bars detection in induction motors. Measurement 2016; 90: 519-525. doi: 10.1016/j.measurement.2016.05.010

[19] Romero-Troncoso RJ, Garcia-Perez A, Morinigo-Sotelo D, Duque-Perez O, Osornio-Rios RA et al. Rotor unbalance and broken rotor bar detection in inverter-fed induction motors at start-up and steady-state regimes by high-resolution spectral analysis. Electric Power Systems Research 2016; 133: 142-148. doi: 10.1016/j.epsr.2015.12.009

[20] Park Y, Choi H, Lee SB, Gyftakis KN. Search coil-based detection of nonadjacent rotor bar damage in squirrel cage induction motors. IEEE Transactions on Industry Applications 2020; 56 (5): 4748-4757. doi: 10.1109/TIA.2020.3000461

[21] Iglesias-Martínez ME, de Córdoba PF, Antonino-Daviu JA, Conejero JA. Detection of nonadjacent rotor faults in induction motors via spectral subtraction and autocorrelation of stray flux signals. IEEE Transactions on Industry Applications 2019; 55 (5): 4585-4594. doi: 10.1109/TIA.2019.2917861

[22] Assaf T, Henao H, Capolino GA. Simplified axial flux spectrum method to detect incipient stator inter-turn short-circuits in induction machine. In: IEEE 2004 International Symposium on Industrial Electronics; Ajaccio, France; 2004. pp. 815-819. doi: 10.1109/ISIE.2004.1571918

[23] Kia SH, Henao H, Capolino GA, Martis C. Induction machine broken bars fault detection using stray flux after supply disconnection. In: IECON 2006 32nd Annual Conference on IEEE Industrial Electronics; Paris, France; 2006. pp. 1498-1503. doi: 10.1109/IECON.2006.347595

[24] Yazidi A, Henao H, Capolino GA, Artioli M, Filippetti F et al. Flux signature analysis: An alternative method for the fault diagnosis of induction machines. In: IEEE 2005 Russia Power Tech; St. Petersburg, Russia; 2005. pp. 1-6. doi: 10.1109/PTC.2005.4524578

[25] Riera-Guasp M, Antonino-Daviu JA, Capolino GA. Advances in electrical machine, power electronic, and drive condition monitoring and fault detection: state of the art. IEEE Transactions on Industrial Electronics 2014; 62 (3): 1746-1759. doi: 10.1109/TIE.2014.2375853

[26] Antonino-Daviu JA, Pons-Llinares J, Shin S, Lee KW, Lee SB. Reliable detection of induction motor rotor faults under the influence of rotor core magnetic anisotropy. In: IEEE 2015 10th International Symposium on Diagnostics for Electrical Machines, Power Electronics and Drives (SDEMPED); Guarda, Portugal; 2015. pp. 14-21. doi: 10.1109/DEMPED.2015.7303663

[27] Akar M, Cankaya I. Broken rotor bar fault detection in inverter-fed squirrel cage induction motors using stator current analysis and fuzzy logic. Turkish Journal of Electrical Engineering & Computer Sciences 2012; 20 (Sup. 1): 1077-1089. doi: 10.3906/elk-1102-1050

[28] Seera M, Lim CP, Ishak D, Singh H. Fault detection and diagnosis of induction motors using motor current signature analysis and a hybrid FMM–CART model. IEEE transactions on neural networks and learning systems 2011; 23 (1): 97-108. doi: 10.1109/TNNLS.2011.2178443

[29] Abid FB, Sallem M, Braham A. Robust interpretable deep learning for intelligent fault diagnosis of induction motors. IEEE Transactions on Instrumentation and Measurement 2019; 69 (6): 3506-3515. doi: 10.1109/TIM.2019.2932162

[30] Gomez-Gil P, Rangel-Magdaleno J, Ramirez-Cortes JM, Garcia-Trevino E, Cruz-Vega I. Intelligent identification of induction motor conditions at several mechanical loads. In: IEEE 2016 International Instrumentation and Measurement Technology Conference Proceedings; Taipei, Taiwan; 2016. pp. 1-5. doi: 10.1109/I2MTC.2016.7520396

[31] Ali MZ, Shabbir MN, Liang X, Zhang Y, Hu T. Machine learning-based fault diagnosis for single-and multi-faults in induction motors using measured stator currents and vibration signals. IEEE Transactions on Industry Applications 2019; 55 (3): 2378-2391. doi: 10.1109/TIA.2019.2895797

[32] Godse R, Bhat S. Combined morphology and SVM-based fault feature extraction technique for detection and classification of transmission line faults. Turkish Journal of Electrical Engineering & Computer Sciences 2020; 28 (5): 2768-2788. doi: 10.3906/elk-1912-7

[33] Bhalja B, Maheshwari RP. Wavelet-based fault classification scheme for a transmission line using a support vector machine. Electric Power Components and Systems 2008; 36 (10): 1017-1030. doi: 10.1080/15325000802046496

[34] LaValle SM, Branicky MS, Lindemann SR. On the relationship between classical grid search and probabilistic roadmaps. The International Journal of Robotics Research 2004; 23 (7-8): 673-692. doi: 10.1177/0278364904045481

[35] Subasi A. Classification of EMG signals using PSO optimized SVM for diagnosis of neuromuscular disorders. Computers in biology and medicine 2013; 43 (5): 576-586. doi: 10.1016/j.compbiomed.2013.01.020

[36] Wu CH, Tzeng GH, Lin RH. A novel hybrid genetic algorithm for kernel function and parameter optimization in support vector regression. Expert Systems with Applications 2009; 36 (3): 4725-4735. doi: 10.1016/j.eswa.2008.06.046

[37] Zhang X, Chen X, He Z. An ACO-based algorithm for parameter optimization of support vector machines. Expert systems with applications 2010; 37 (9): 6618-6628. doi: 10.1016/j.eswa.2010.03.067

[38] Rao RV, Savsani VJ, Vakharia DP. Teaching–learning-based optimization: a novel method for constrained mechanical design optimization problems. Computer-Aided Design 2011; 43 (3): 303-315. doi: 10.1016/j.cad.2010.12.015

[39] Torrence C, Compo GP. A practical guide to wavelet analysis. Bulletin of the American Meteorological society 1998; 79 (1): 61-78. doi: 10.1175/1520-0477(1998)079<0061:APGTWA>2.0.CO;2

[40] Pan YN, Chen J, Li XL. Spectral entropy: a complementary index for rolling element bearing performance degradation assessment. Proceedings of the Institution of Mechanical Engineers, Part C: Journal of Mechanical Engineering Science 2009; 223 (5): 1223-1231. doi: 10.1243/09544062JMES1224

[41] Luan Y, Huang Y, Zheng X, Cheng J. Seismic time-frequency analysis based on entropy-optimized Paul wavelet transform. IEEE Geoscience and Remote Sensing Letters 2019; 17 (2): 342-346. doi: 10.1109/LGRS.2019.2919756

[42] Cohen MX. A better way to define and describe Morlet wavelets for time-frequency analysis. NeuroImage 2019; 199: 81-86. doi: 10.1016/j.neuroimage.2019.05.048

[43] Yang DJ, Liu RF, Hu MQ. Transient starting performance of squirrel cage induction motor with time-stepping FEM. Electric Machines and Control 2003; 7 (3): 177-181 .

[44] Aydin I, Karakose M, Akin E. An approach for automated fault diagnosis based on a fuzzy decision tree and boundary analysis of a reconstructed phase space. ISA transactions 2014; 53 (2): 220-229. doi: 10.1016/j.isatra.2013.11.004

[45] Zhao W, Wang L. Multiple-kernel MRVM with LBFO algorithm for fault diagnosis of broken rotor bar in induction motor. IEEE Access. 2019; 7: 182173-182184. doi: 10.1109/ACCESS.2019.2958689

[46] Ferrucho-Alvarez ER, Martinez-Herrera AL, Cabal-Yepez E, Rodriguez-Donate C, Lopez-Ramirez M et al. Broken Rotor Bar Detection in Induction Motors through Contrast Estimation. Sensors 2021; 21 (22): 7446. doi: 10.3390/s21227446

[47] Rangel-Magdaleno J, Peregrina-Barreto H, Ramirez-Cortes J, Cruz-Vega I. Hilbert spectrum analysis of induction motors for the detection of incipient broken rotor bars. Measurement 2017; 109: 247-255. doi: 10.1016/j.measurement.2017.05.070